J. Cent. South Univ. (2022) 29: 693−711
DOI: https://doi.org/10.1007/s11771-022-4946-4

Springer

Characteristics of microseismic *b*-value associated with rock mass large deformation in underground powerhouse caverns at different stress levels

LI Biao(李彪)[1, 2], DING Quan-fu(丁泉富)[1], XU Nu-wen(徐奴文)[3],
DAI Feng(戴峰)[3], XU Yuan(许媛)[4]*, QU Hong-lue(曲宏略)[1]

1. School of Geoscience and Technology, Southwest Petroleum University, Chengdu 610500, China;
2. State Key Laboratory of Explosion Science and Technology, Beijing Institute of Technology, Beijing 100081, China;
3. State Key Laboratory of Hydraulics and Mountain River Engineering, College of Water Resource and Hydropower, Sichuan University, Chengdu 610065, China;
4. Department of Engineering Science, University of Oxford, OX5 1PF, United Kingdom

© Central South University 2022

Abstract: Rock mass large deformation in underground powerhouse caverns has been a severe hazard in hydropower engineering in Southwest China. During the development of rock mass large deformation, a sequence of fractures was generated that can be monitored using microseismic (MS) monitoring techniques. Two MS monitoring systems were established in two typical underground powerhouse caverns featuring distinct geostress levels. The MS *b*-values associated with rock mass large deformation and their temporal variation are analysed. The results showed that the MS *b*-value in course of rock mass deformation was less than 1.0 in the underground powerhouse caverns at a high stress level while larger than 1.5 at a low stress level. Prior to the rock mass deformation, the MS *b*-values derived from both the high-stress and low-stress underground powerhouse caverns show an incremental decrease over 10% within 10 d. The results contribute to understanding the fracturing characteristics of MS sources associated with rock mass large deformation and provide a reference for early warning of rock mass large deformation in underground powerhouse caverns.

Key words: underground powerhouse caverns; rock mass large deformation; stress level; microseismic monitoring; *b*-value

Cite this article as: LI Biao, DING Quan-fu, XU Nu-wen, DAI Feng, XU Yuan, QU Hong-lue. Characteristics of microseismic *b*-value associated with rock mass large deformation in underground powerhouse caverns at different stress levels [J]. Journal of Central South University, 2022, 29(2): 693−711. DOI: https://doi.org/10.1007/s11771-022-4946-4.

1 Introduction

In underground powerhouse caverns, a step increase of rock mass displacement on the order of millimetres or tens of millimetres occurring within several days or weeks is generally recognised as large deformation. Rock mass large deformation, if without intervention or control, may lead to visible failures such as collapses and rock slide. Rock mass deformation induced by excavation unloading of large underground powerhouse caverns threatens the

Foundation item: Projects(51809221, 51679158) supported by the National Natural Science Foundation of China; Project(KFJJ20-06M) supported by the State Key Laboratory of Explosion Science and Technology (Beijing Institute of Technology), China
Received date: 2020-07-22; **Accepted date:** 2021-04-07
Corresponding author: XU Yuan, PhD, Research Associate; Tel: +44-077-84089735; E-mail: yuan.xu@eng.ox.ac.uk; ORCID: https://orcid.org/0000-0002-5814-2357

safety of personnel and equipment under construction and has adverse impact during normal operations, which has been a significant issue during the construction of the hydropower projects in Southwest China. Hence, it is of great significance to identify the potential deformation zone, to understand the deformation mechanisms and to conduct a real-time warning of underground surrounding rocks. Over the past few decades, the microseismic (MS) monitoring technique has been applied to establish the relationship between rock fractures (MS events) and rock mass deformation in geotechnical engineering projects such as mines [1−3], underground oil and gas storage [4], carbon dioxide sequestration [5], nuclear waste repositories [6, 7] and hydropower stations [8 − 12]. Abundant rock fracturing information such as magnitude, energy and apparent stress of the located MS events can be obtained using the MS monitoring technique. Magnitude has been the most pervasive measure of seismic intensity. The magnitude-frequency relationship of MS events reflects the characteristics of fracturing scales in the failure process of rock mass [13]. Thus, it is significant to study the magnitude-frequency relationship of MS events for a better understanding of rock mass large deformation.

The magnitude-frequency characteristics were firstly studied in seismology. Since 1944, GUTENBERG et al [14] had studied the magnitude-frequency characteristics of the seismic events for more than twenty years in the California-Nevada region and proposed the well-known G-R law, expressed as:

$$\lg N=a-bm_{\mathrm{M}} \tag{1}$$

where m_{M} is the magnitude, N is the event count whose magnitude is no less than m_{M}, a and b are constants for the given statistical data and can be acquired by the $\lg N-m_{\mathrm{M}}$ diagram. The parameter b, also called b-value, represents the proportion of high and low magnitude of events. Large b-values usually mean low-magnitude events are dominant while small b-values indicate high-magnitude events occurred more frequently. Due to a clear physical relation with the seismic source, the moment magnitude is widely adopted. The widely used formula to calculate the moment magnitude m_{M} is formally defined as [15]:

$$m_{\mathrm{M}}=\frac{2}{3}\left(\lg M_0-9.1\right) \tag{2}$$

where M_0 is the seismic moment. It is observed that the moment magnitude can be directly calculated by seismic moment, which is a basic parameter to quantify the strength of the seismic event that is model-independent and can be expressed as [16]:

$$M_0=\frac{4\pi\rho c^3 R\Omega_0}{F_{\mathrm{c}}} \tag{3}$$

where ρ represents the density of the source material, c is either P-wave or S-wave velocity, R is the hypocentral distance, Ω_0 is low frequency amplitude of the displacement spectrum of distant seismicities and F_{c} represents the radiation coefficient. The validity of the calculated results has been verified for earthquakes. Theoretically, the moment magnitude has no upper or lower limit and is usually used to reflect the strength characteristics of engineering microseismicities, the moment magnitude of which is almost less than 3.0 [8, 17].

The b-value of natural seismicity has been researched for many years since the G-R law was put forward. Through exploring the spatial variations of b-values, some researchers [18 − 20] pointed out that along fault zones the low b-values seemed to correspond with asperities while high b-values were related to creeping sections of faults. Moreover, the relationships were revealed between b-values and other parameters such as faulting style [21], earthquake depth [22] and seismic moment or stress [23−25]. KULHANEK et al [26] analysed the temporal variations of b-values of seismic events in the shallow subduction zones of Cocos and Nazca plates and found that significant drops in b-values might occur when preceding large earthquakes.

Much attention has been paid to the MS b-value to reveal the fracturing scales of the rock mass in an increasing number of engineering projects over last few years. LEGGE et al [27] evaluated spatial characteristics of b-values of mining-induced MS events and found that low b-values were potentially induced by MS events distributed in two dimensions, while high b-values might be resulted from three-dimensional failures. Through analysing the magnitude-frequency characteristics of MS events during mining, HUDYMA et al [13] discovered that the b-values were commonly low for the MS events induced by

fault activation and high *b*-values of MS events were the result of the local stress change immediately following blasts. Some studies have found that prior to large seismic events in mines (such as rockbursts, and roof collapses), the *b*-values showed a gradual tendency to decrease [28–30].

Previous research into the MS *b*-value has shown its favorable potential for delivering important information on possible hazards in a region. In the present study, in the context of two typical underground powerhouse caverns at different stress levels in Southwest China, the *b*-values associated with rock mass large deformation were extracted, and the characteristics of the *b*-value with regard to the stress level was investigated. The temporal variation of the *b*-value was revealed during rock mass large deformation, which contributes to laying the foundation for the early warning of large deformation hazards of rock mass in underground powerhouse caverns.

2 MS monitoring data

2.1 High stress underground powerhouse caverns of Houziyan Hydropower Project

2.1.1 Engineering background

The Houziyan Hydropower Project was constructed on the Dadu River in Sichuan Province, China. The underground powerhouse caverns were designed in the right bank mountain, with a total installed capacity of 1700 MW. The underground powerhouse caverns mainly include the main powerhouse, the main transformer chamber, and the tailrace surge chamber (Figure 1). The caverns were excavated by layer and their excavation sizes are

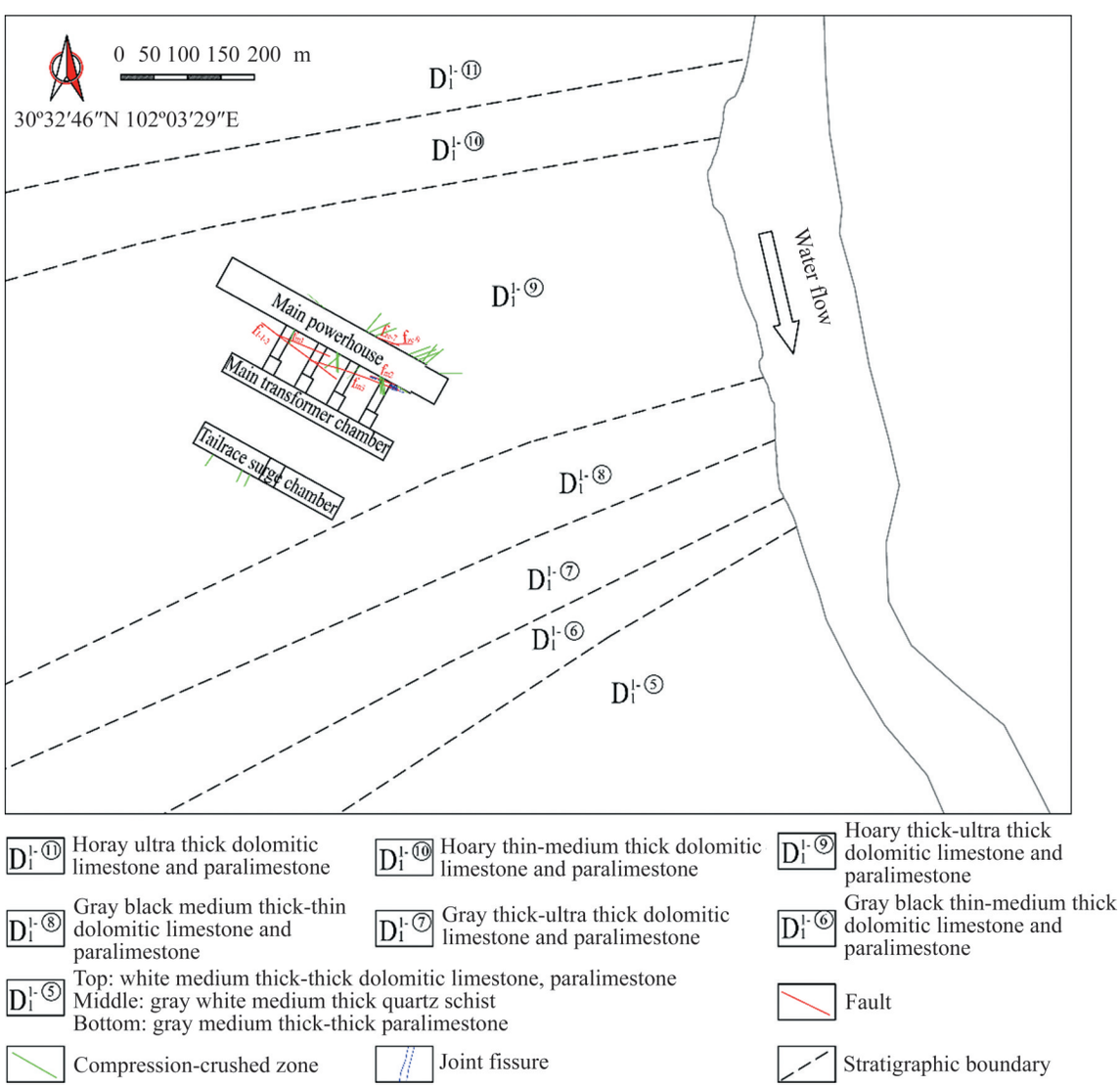

Figure 1 Geological plane of underground powerhouse caverns of Houziyan Hydropower Project

219.5 m×29.2 m×68.7 m (length×width×height), 139 m×18.80 m×25.2 m (length×width×height), and 140.5 m×23.5 m×75.0 m (length×width×height), respectively.

The terrain in both sides of the valley is steep and the heights of the slopes near the valley are more than 800 m. The topographic slope of the right bank is 45°–60°. The underground powerhouse is buried at a depth of 280–510 m horizontally and 400–660 m vertically. As shown in Figure 1, dolomitic limestone and metamorphic limestone of the lower Devonian are the main components of the rock mass in the underground powerhouse caverns and their attitudes are 320°–340°/∠25°–50° (320°–340°: dip direction; ∠25°–50°: dip angle). The quality of the rock mass is classified taking into account three primary factors (i.e., rock strength, rock mass integrity and structural plane conditions) and two secondary factors (i.e., underground water and orientations of structural planes). An intermediate quality of the rock mass in Houziyan underground powerhouse is identified as it mainly comprises Class III rock while with Class IV rock exposed locally [31]. The geostresses of the underground powerhouse caverns were tested using borehole stress relief method (also called overcoring method, one of the the suggested methods for rock stress estimation by the International Society for Rock Mechanics, ISRM) [32, 33]. Six points in different areas of the underground caverns were tested. The results show that the maximum principal geostress in the underground powerhouse caverns is 21.46–36.43 MPa. The rock mass strength-to-stress ratio is only 2–4, which indicates that the Houziyan underground powerhouse is a typical high geo-stress example of large hydropower projects [34]. During the excavation of the caverns, weak rockbursts and rock failures occurred at times.

2.1.2 MS monitoring system

An MS monitoring system was established to monitor the evolution process of microfractures during the rock mass deformation of the underground powerhouse caverns. Sixteen accelerometers (including fifteen uniaxial accelerometers and one triaxial accelerometer) were installed by grouting at the end of diamond-drilled boreholes in the rock mass of the layer drainage galleries and the upstream sidewall of the main transformer chamber, as shown in Figure 2. The

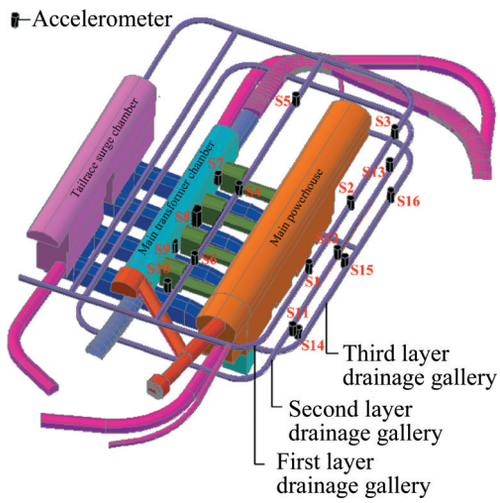

Figure 2 Spatial layout of accelerometers of Houziyan underground powerhouse caverns

frequency response of the uniaxial accelerometers is 50 Hz–5 kHz and the sensitivity is 30 V/g. The frequency response in x, y and z directions of the triaxial accelerometer is 0.13 Hz–8 kHz, and the sensitivities are 1.4 V/g in x, y directions and 1.6 V/g in z direction. The sampling frequency of the digital signal acquisition station is 10 kHz. The waveforms are recorded automatically in the Hyperion digital signal processing system once the STA/LTA is larger than 3. The monitoring system almost covers the crown zone, the upstream and downstream sidewalls of the main powerhouse, and the rock pillar between the main powerhouse and the main transformer chamber. The signals captured by the accelerometers are transported to the Paladin digital signal acquisition system using copper twisted-pair cables. Through fixed-point blasting tests and back analysis, the P-wave velocity of rock mass was determined as 5700 m/s. Given the installed locations of accelerometers and the P-wave velocity of rock mass, a time difference between the actual arrival and theoretical arrival can be calculated by assuming the MS location and occurrence time. Then the MS location can be iteratively approximated by minimizing the sum of the time difference calculated by multiple accelerometers.

There are various signals in the underground powerhouse and each signal has its special time-frequency characteristics, and the MS events can be identified through time-frequency analysis. Because the excavation areas of the underground caverns are

not far from the sensors and the explosives are of high energies, the amplitudes of blasting waveforms are usually large. Therefore, as a simple and quick method, the amplitude and attenuation of different signals are usually used for identification of different signals. To better analyse the frequencies of signals, the S-transform time-frequency method was used to obtain the dominant frequencies of different signals [35]. Figure 3 illustrates typical waveforms of different signals recorded in

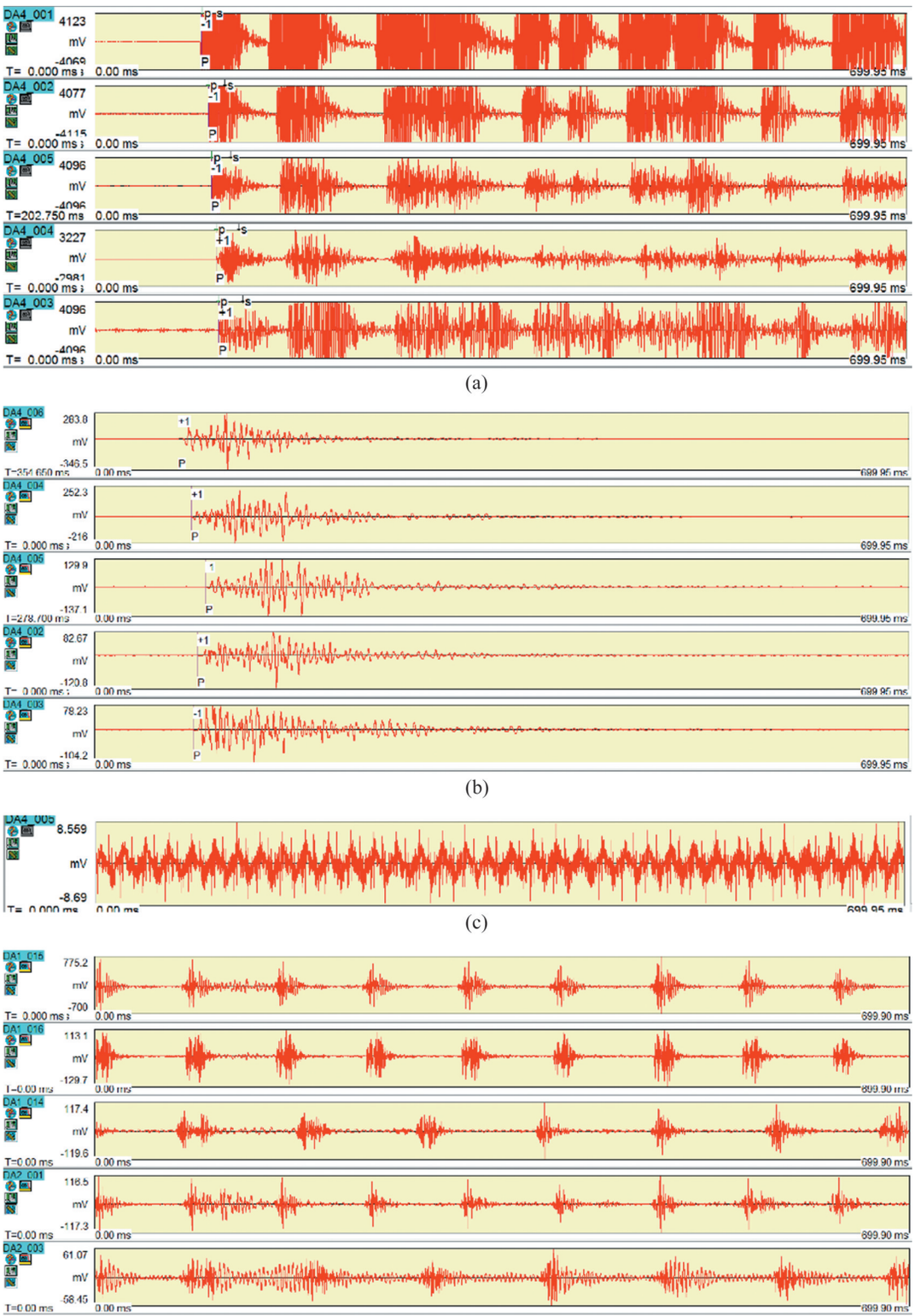

Figure 3 Typical waveforms of different signals in underground powerhouse caverns: (a) Blasting event; (b) MS event; (c) Electric signal; (d) Mechanical vibration

Houziyan underground powerhouse caverns. The blasting waveforms have large amplitudes, and there are usually several regular waveforms in a window (Figure 3(a)). The frequency of blasting waveforms is always high with the value between 500 and 100 Hz. The amplitudes of MS signals are almost dozens to hundreds milivolt and they have lower frequencies with the value of dozens to 400 Hz. Besides, the waveforms attenuate slowly (Figure 3 (b)). The electric signals have a constant frequency about 50 Hz (Figure 3(c)). The mechanical vibration signals usually have several similar waveforms in a window and the peak amplitudes are less than 1000 mV (Figure 3(d)).

2.2 Low stress underground powerhouse caverns of Wudongde Hydropower Project

2.2.1 Engineering background

The Wudongde Hydropower Project is under construction on the Jinsha River between Sichuan and Yunnan Provinces, China. The underground powerhouse caverns were respectively designed in the left and right banks. Six units will be installed in the underground powerhouse caverns of each bank, with a total capacity of 10200 MW. Main underground caverns include the main powerhouse, the main transformer chamber and three tailrace surge chambers (Figure 4). These caverns were excavated by layer and the excavation sizes are

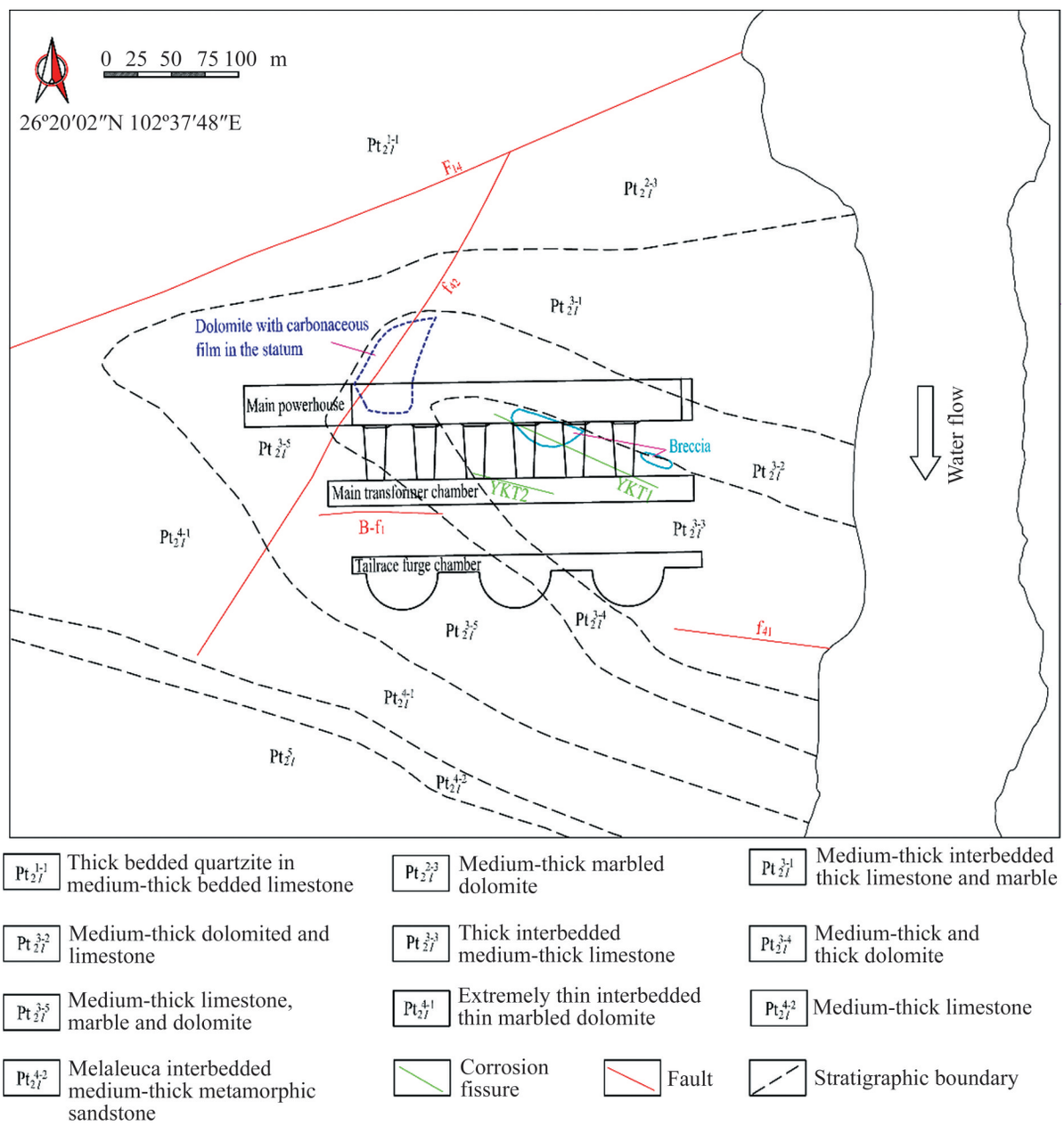

Figure 4 Geological plane of underground powerhouse caverns of Wudongde Hydropower Project

respectively 333.00 m×30.50 m×89.80 m (length×width×height), 272.00 m×18.80 m×35.00 m (length×width×height), and 25.00 m×113.50 m (diameter×height).

The valley is narrow and steep, and almost symmetrical on both sides. The topographic slope of the banks is 60°−75°. The buried depths of the underground powerhouse are 100 − 120 m horizontally and 180−390 m vertically. As shown in Figure 4, the rock mass mainly consists of limestone, dolomite, quartzite and griotte of the Sinian system. The attitudes of the strata change greatly from the shallow to the deep. Close to the river and in the middle section, the attitude of the strata is 155°−185°/∠70°−85°, while it is 15°−40°/∠60°−75° inside the mountain. The rock mass is mainly composed of Classes II and III, which means that the rock mass quality is intermediate to relatively well. The geostresses of the underground powerhouse caverns were tested using the ISRM suggested methods for rock stress estimation, borehole stress relief method [32, 33] and hydraulic fracturing method [36]. Totally ten points were tested to obtain the geostress of the underground caverns. The results reveal that the maximum principal geo-stress is between 5.0 MPa and 11.5 MPa, almost in the vertical direction [37]. The rock mass strength-to-stress ratio is 7.4−17.0, which is relatively high. In such a low stress underground engineering, the shapes of the caverns were well formed during excavation and no rockbursts and large failures occurred.

2.2.2 MS monitoring system

To reveal the evolution process of microfractures during the rock mass deformation, an MS monitoring system was introduced to the underground powerhouse caverns. Eighteen accelerometers with the frequency response of 50 Hz−5 kHz were installed in the upstream second layer drainage gallery, the downstream sidewall of the main powerhouse and the omnibus bar caves, as shown in Figure 5 [38]. The sensitivity of the accelerometers is about 30 V/g. The digital signal acquisition station has a sampling frequency of 10 kHz. The crown zone, the upstream and downstream sidewalls of the main powerhouse, and the rock pillar between the main powerhouse and the main transformer chamber are the main monitoring regions. The P-wave velocity of rock mass was determined as 5000 m/s [39]. The same setting was adopted as in Houziyan underground powerhouse for the connection of the system, data acquisition and signal analysis.

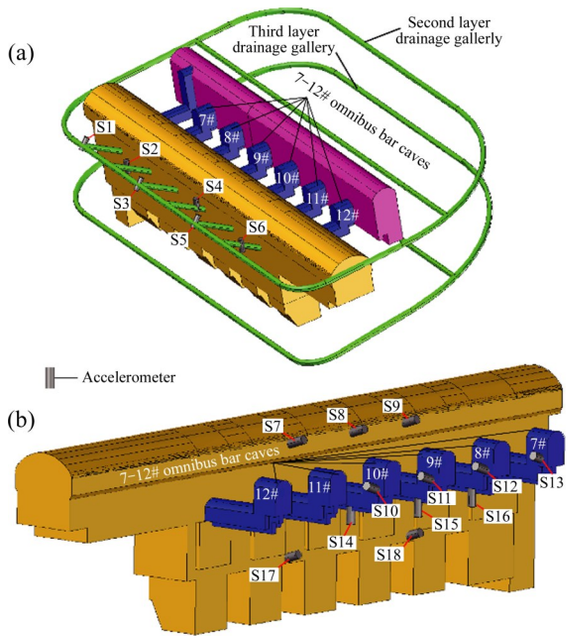

Figure 5 Spatial layout of accelerometers of Wudongde underground powerhouse caverns: (a) Upstream sidewall; (b) Downstream sidewall areas [38]

3 *b*-values associated with rock mass large deformation

3.1 Calculating results of *b*-values

The minimum magnitude of complete recording events, M_c, is a significant parameter for most seismic studies. As a fast and reliable estimate method of M_c, the point of the maximum curvature is defined as magnitude of completeness by computing the maximum value of the first derivative of the frequency − magnitude curve [40]. In practice, this matches the magnitude bin with the highest frequency of events in the non-cumulative frequency-magnitude distribution and this method is adopted to determine M_c in our study. Based on the frequency-magnitude distribution of MS events with the magnitude larger than M_c, the accumulative generalised linear regression model (GLM) assuming Poisson errors was adopted to provide a good fit to frequency-magnitude data for natural

seismicity and rock AE [41, 42].

3.1.1 High stress underground powerhouse caverns

The MS monitoring system had been in operation since April 12, 2013, when the fourth bench of the main powerhouse was to be excavated. Myriads of MS events induced by excavation unloading were acquired in the Houziyan underground powerhouse caverns. During the MS monitoring period, the downstream sidewall of the main powerhouse was the main deformation region. Four rock mass large deformation problems corresponding to MS clusters are shown in Figure 6. It can be seen from the absolute displacement process diagram of multipoint extensometers that the rock mass large deformation had obvious step increments and the increasing values of the displacements of rock mass excavation surfaces were respectively 9.89 mm, 6.35 mm, 7.90 mm, and 18.54 mm. A few days before and during the rock mass deformation, the MS events accumulated around the deformation regions (Figure 6). Thus, it can be verified that rock mass large deformation has a close relation with MS activities.

The MS *b*-values calculated in Figure 7 correspond to the MS clusters in Figure 6. According to Eq. (1), we obtain statistics for m_M and N. The cumulative least-square fit is then implemented with m_M as the x-coordinate and lg$N$ as the y-coordinate. The slope of this straight line is the b-value. The coefficients of determination (R^2) are more than 0.94, which demonstrate that the b-value obtained by the liner fitting can reflect the overall proportion of large- and small-magnitude MS events. The *b*-values associated with four rock mass large deformation problems in the Houziyan underground powerhouse are respectively 0.8974, 0.9127, 0.9156 and 0.9952. All of them are less than 1.0 and relatively low.

3.1.2 Low stress underground powerhouse caverns

The MS monitoring system was established on July 7, 2015. The monitoring period covers VI−XI bench excavation of the main powerhouse. Though the Wudongde underground caverns are located in low stress mountain, the rock mass large deformation occurs at times. Four rock mass large deformation problems in the MS clustering region are presented in Figure 8. Obvious step increments of rock mass large deformation were observed through the absolute displacement process diagram of multipoint extensometers in this figure. The displacement increments of rock mass excavation surfaces were 11.46, 5.41, 3.24 and 5.95 mm, respectively. Similar to the MS evolution in high stress underground caverns, the MS events also accumulated in the deformation regions before and during the rock mass deformation (Figure 8). The magnitudes of the MS events are generally lower than the Houziyan underground powerhouse caverns.

Corresponding *b*-values of MS clusters associated with four rock mass large deformation problems described above (Figure 8) are shown as Figure 9. The *b*-values associated with four rock mass large deformation problems in the Wudongde underground powerhouse caverns are respectively 1.7709, 1.5489, 2.0507 and 1.5193, which are larger than those characterized in the Houziyan underground powerhouse caverns. The *b*-values associated with rock mass large deformation in high stress underground caverns are less than 1.0 but more than 1.5 in low stress underground caverns. As shown in Eq. (1), small *b*-values usually reflect that high-magnitude events occurred more frequently while large *b*-values statistically indicate that low-magnitude events are dominant. This indicates that in high stress underground caverns, high-magnitude MS events occurred more frequently while low-magnitude MS events are dominant in low stress underground caverns.

3.2 Temporal variations of *b*-values during development of rock mass large deformation

The temporal variations of *b*-values during the development of rock mass large deformation in the Houziyan and the Wudongde underground caverns are shown in Figures 10 and 11. During the process of rock mass deformation, the *b*-values in high stress underground caverns are smaller than those in low stress underground caverns, which is consistent with the general characteristics of *b*-values outlined above. However, the *b*-values saw a decreasing trend in both high stress and low stress underground caverns prior to the rock mass large deformation. The temporal variation of the *b*-values along with the absolute displacement is further detailed in Tables 1 and 2. The *b*-value and absolute

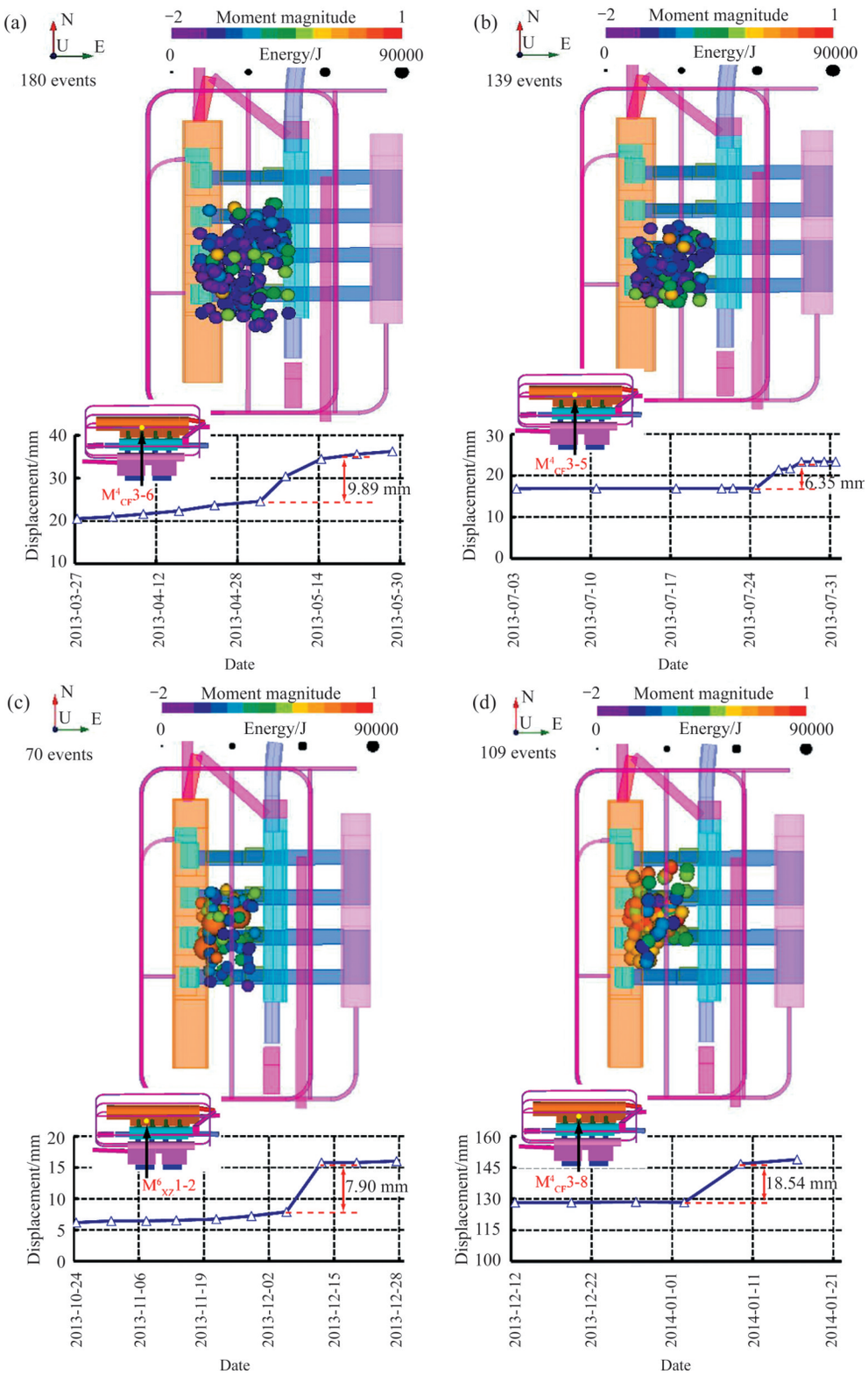

Figure 6 Rock mass large deformation in MS clustering region of the Houziyan underground powerhouse caverns: (a) MS cluster recorded from April 16, to May 20, 2013 and the absolute displacement process diagram of multipoint extensometer M^4_{CF}3-6 (Stake 0 + 51.3 m, EL 1721.2 m); (b) MS cluster recorded from July 4 to July 28, 2013 and the absolute displacement process diagram of multipoint extensometer M^4_{CF}3-5 (Stake 0 + 51.3 m, EL 1723.2 m); (c) MS cluster recorded from November 10, to December 15, 2013 and the absolute displacement process diagram of multipoint extensometer M^6_{XZ}1-2 (Stake 0 + 34.0 m, EL 1705.4 m); (d) MS cluster recorded from December 12, 2013 to January 10, 2014 and the absolute displacement process diagram of multipoint extensometer M^4_{CF}3-8 (Stake 0+51.3 m, EL 1706.5 m)

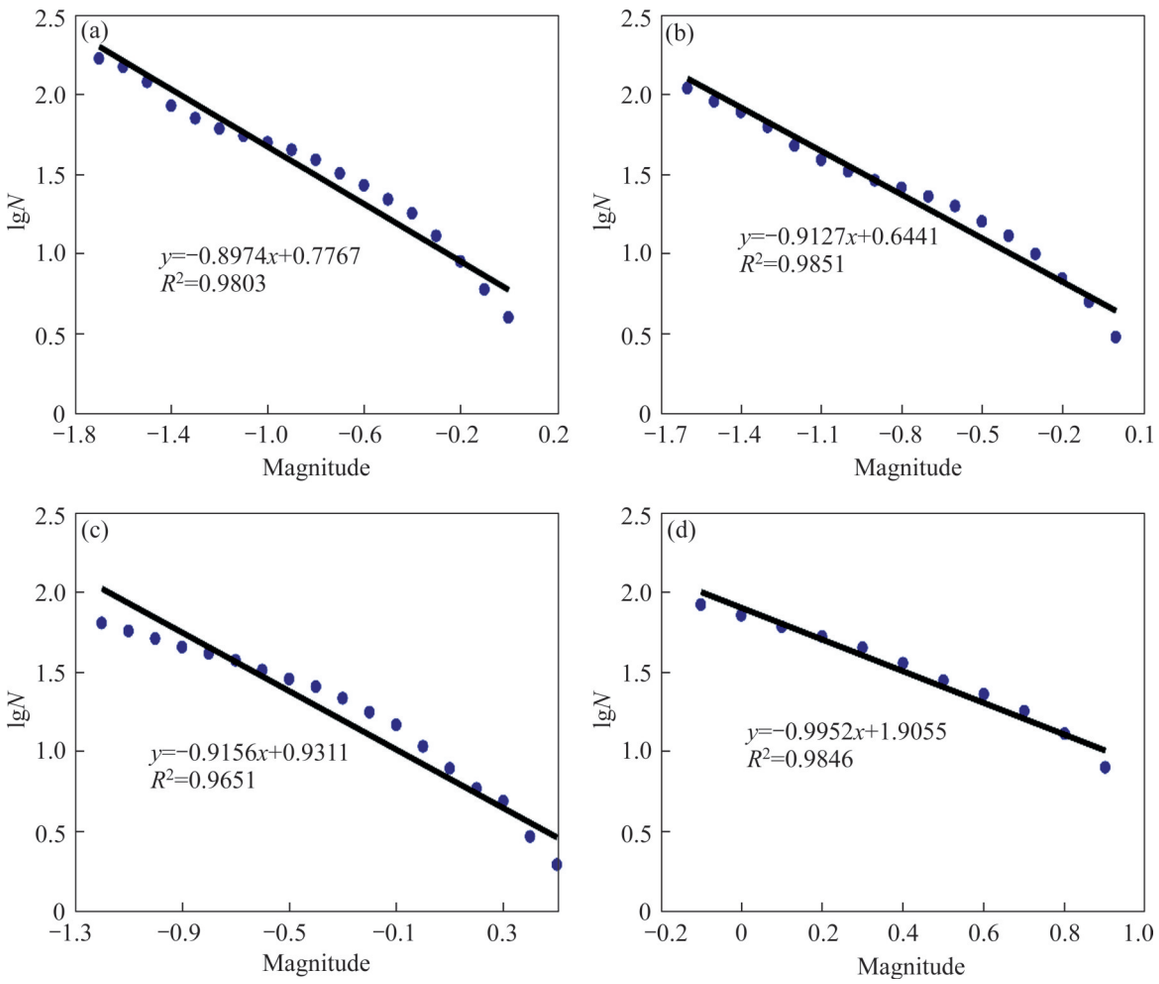

Figure 7 *b*-values of MS clusters associated with rock mass large deformation of in the Houziyan underground caverns ((a), (b), (c) and (d) are the calculating results respectively corresponding to (a), (b), (c) and (d) in Figure 6)

displacement obtained ten days before the rock mass large deformation were regarded as the reference and the amount of relative increments is assessed herein. It can be concluded from all the cases in Tables 1 and 2 that the incremental decrease of *b*-value with respect to the reference point was more than − 10% one day before rock mass large deformation. The rock mass large deformation occurred in an abrupt manner, as indicated by the neglectable amount of incremental increase of the absolute displacement before large deformation, taking the rock mass large deformation occurring from May 2 to May 20, 2013 for example, as shown in Figure 10(a) and Table 1. Ten days before rock mass large deformation, the *b*-value was 1.0420 and the absolute deformation was 23.68 mm. Five days before rock mass large deformation, the *b*-value was 0.8969 and the absolute displacement was still 23.68 mm. The incremental decrease of *b*-value was −0.145 and more than −14%. One day before rock mass large deformation, the *b*-value was 0.8587 and the absolute deformation was 24.60 mm. The incremental decrease of *b*-value was − 0.183 and more than −18%. During the large deformation, the *b*-value was 0.8209 and the incremental decrease was −0.221 and −21%, while the absolute displacement was 34.69 mm, with the incremental increase of 10.81 mm. This decreasing feature of the *b*-value comes with valid interpretations that before rock mass large deformation, an increasing number of cracks in the rock mass initiated, propagated, and coalesced, resulting in increasing high-magnitude MS events. In this regard, the temporal variation of the *b*-value can be employed as a significant index for early warning of rock mass large deformation in underground powerhouse caverns. An incremental decrease over 10% of the *b*-value within ten days can work as an alert. However, it can be seen from

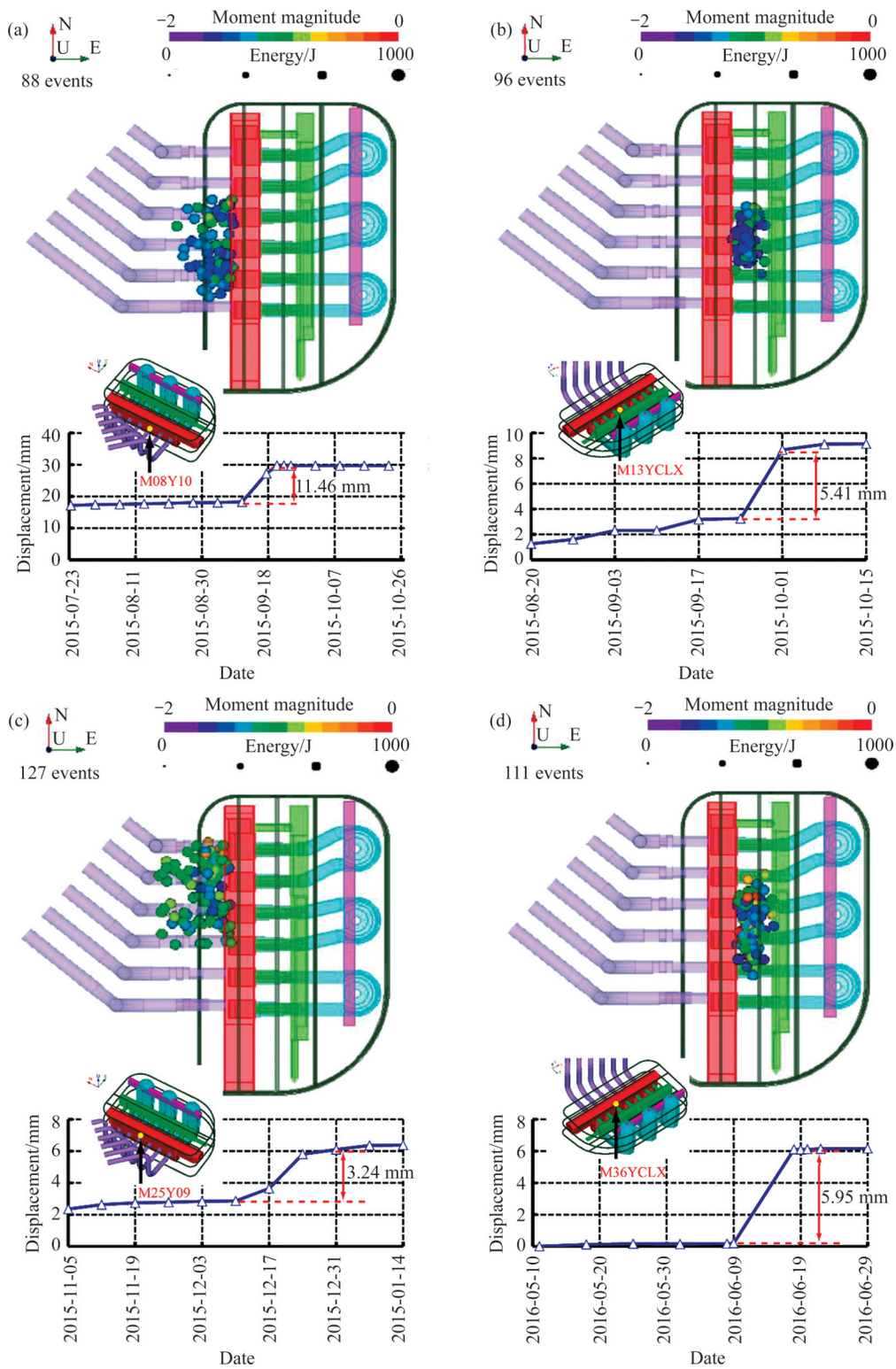

Figure 8 Rock mass large deformation in MS clustering region of the Wudongde underground powerhouse caverns: (a) MS cluster recorded from August 1, to September 20, 2015 and the absolute displacement process diagram of multipoint extensometer M08Y10 (Stake 1 + 172.50 m, EL 812.35 m); (b) MS cluster recorded from August 20, to September 30, 2015 and the absolute displacement process diagram of multipoint extensometer M13YCLX (Stake 1 + 186.00 m, EL 817.75 m); (c) MS cluster recorded from November 11, to December 31, 2015 and the absolute displacement process diagram of multipoint extensometer M25Y09 (Stake 1 + 223.85 m, EL 823.80 m); (d) MS cluster recorded from May 10, to June 25, 2016 and the absolute displacement process diagram of multipoint extensometer M36YCLX (Stake 1 + 174.50 m, EL 849.85 m)

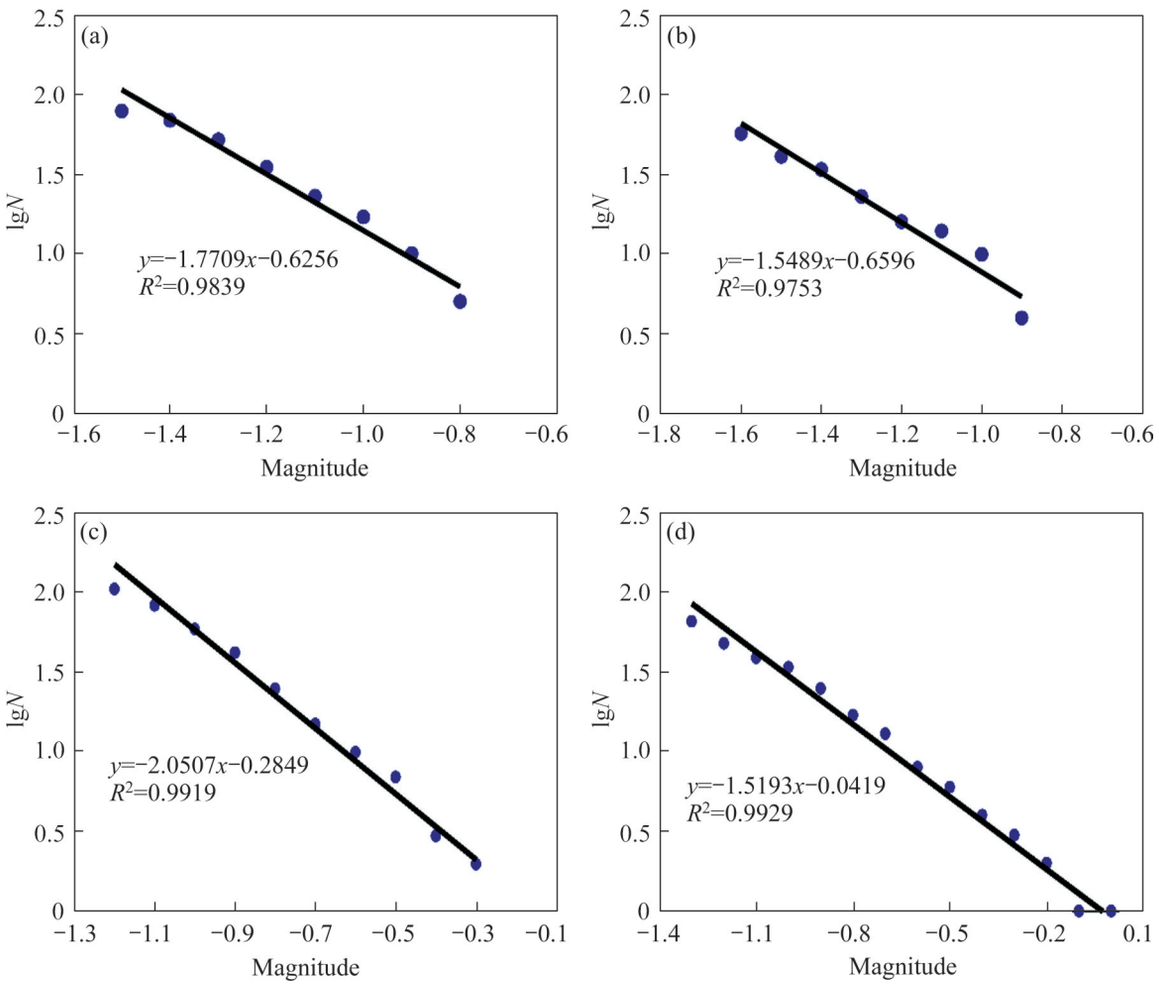

Figure 9 *b*-values of MS clusters associated with rock mass large deformation of in the Wudongde underground caverns ((a), (b), (c) and (d) are the calculating results respectively corresponding to (a), (b), (c) and (d) in Figure 8)

Tables 1 and 2 that the amount of rock mass large deformation varies from several millimetres to tens of millimetres. The available monitoring data are yet insufficient to quantify a conclusive relationship between the *b*-value and the large deformation since rock mass deformation is a complex result of multiple geotechnical factors including the rock quality, the excavation size and type, the geostress tensor, the initial deformation, etc [9, 39, 43, 44].

4 Discussion

Rock mass large deformation induced by excavation has been a critical problem during the construction of the underground caverns in many hydropower projects. This hazard occurs in regions at either high or low geo-stress levels, and adversely affects the construction process. The present study focuses on the magnitude-frequency characteristics of the MS events and demonstrates the importance and reliability of the real-time MS *b*-value as a precursor of rock mass large deformation, in the light of (a) the nature of the microseismicity related to the microfracturing in rock mass; (b) the accessibility of the *b*-value thanks to the rapidly developing monitoring and analysing techniques; (c) the correlation between the absolute *b*-value and the geostress; and (d) the temporal variation of the *b*-value as an indicator of impending rock mass large deformation.

Microseismicity is an inherent feature of rock mass when cracks, fractures or failures occur. This feature enables quantitative assessment of damage in rock at either on-site or laboratory scale [6, 7, 45, 46]. As an important parameter describing the magnitude-frequency relationship of seismic events, the *b*-value of the G-R law has shown its potential to deliver revealing and predictive information

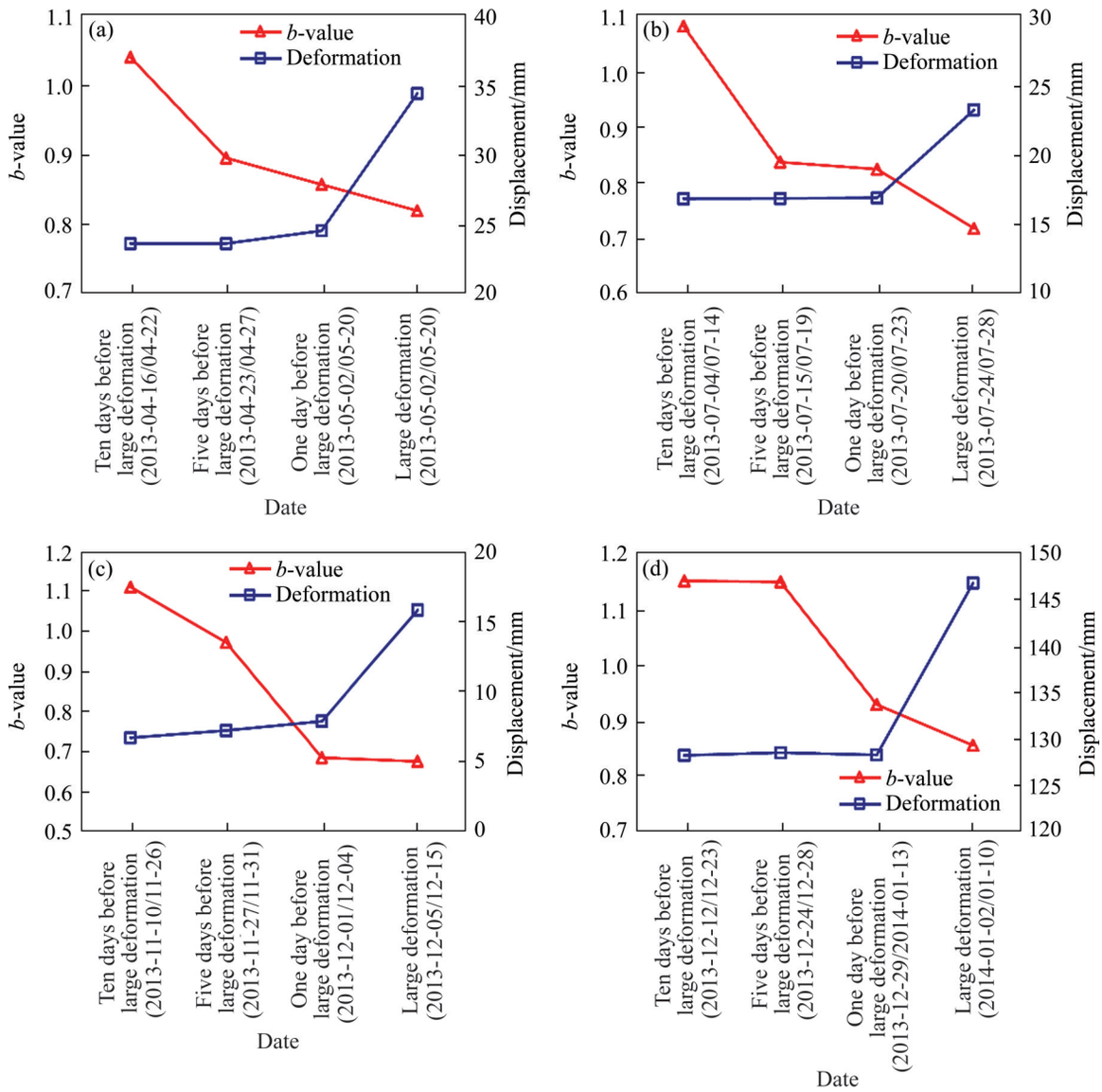

Figure 10 Evolution of *b*-values during the development of rock mass large deformation in the Houziyan underground caverns ((a), (b), (c) and (d) are the calculating results respectively corresponding to (a), (b), (c) and (d) in Figure 6)

of fault activation [13, 18 − 20], earthquake [26], rockburst [28 − 30], etc. in terms of its spatial and temporal variations.

A range of studies have been implemented to develop and improve the techniques of monitoring, recognizing, sampling and analysing the seismic and MS sequences [47, 48]. In particular, the time-frequency analysis enables the recognition of the MS sequences from different types of events, such as artificial blasting events, mechanical vibrations, in terms of their distinctive frequency spectral characteristics. However, further attention in practice should be paid to noise filtering, first picking of P-wave, and non-uniform rock mass velocities.

The statistical analysis of the *b*-value in the two underground caverns featuring high and low geostress showed that the magnitude of MS events is correlated to the geostress and that, in turn, the absolute *b*-value is able to reflect the geostress level. Over a period before and during large deformation, the *b*-value of MS events is generally smaller in regions at a higher geostress level than that at a lower level. This indicates a larger proportion of high-magnitude events in high-stress regions than that in low-stress regions, which is in good agreement with the comparably larger amount of energy accumulated within the rock mass in

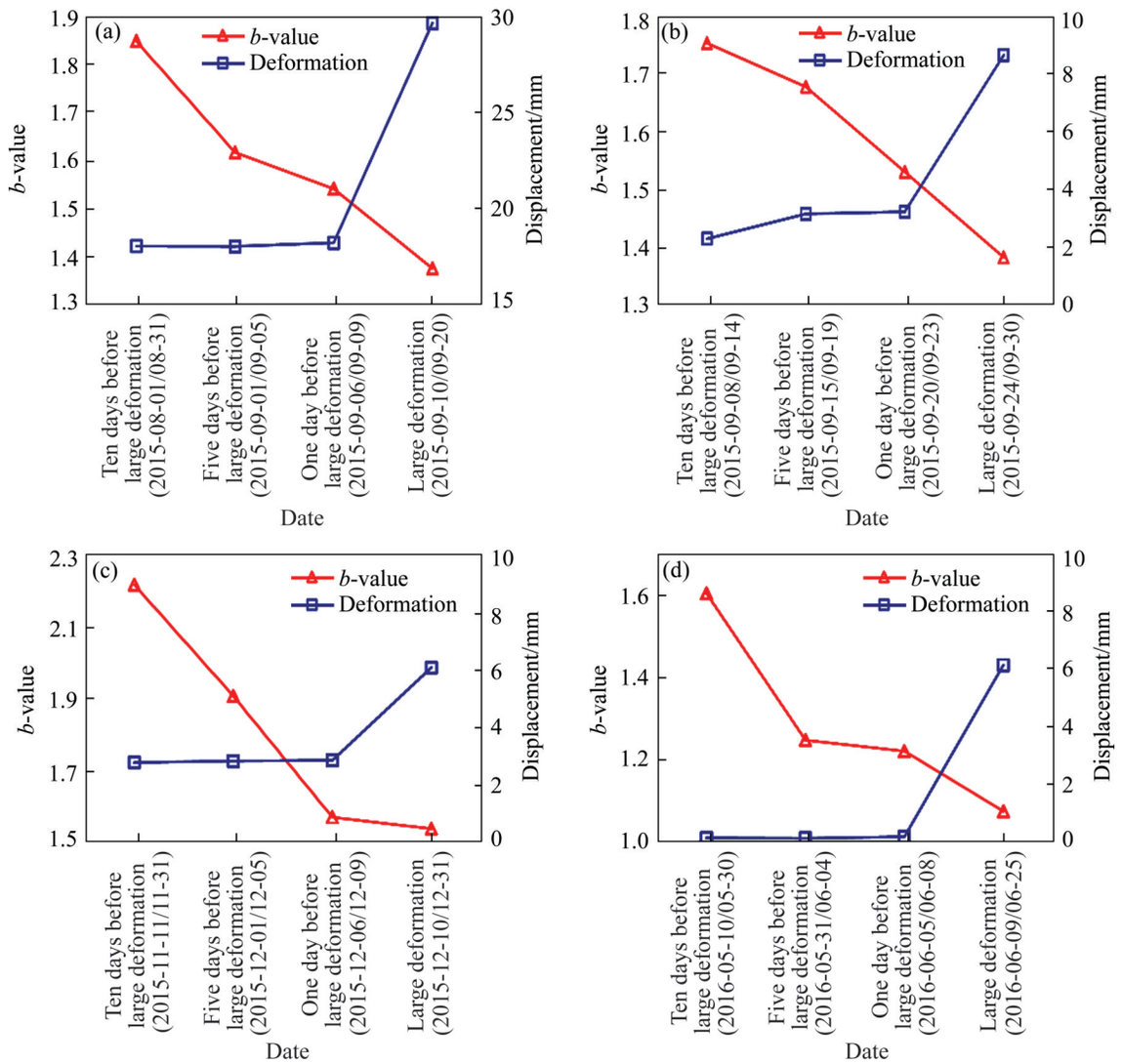

Figure 11 Evolution of *b*-values during the development of rock mass large deformation in the Wudongde underground caverns ((a), (b), (c) and (d) are the calculating results respectively corresponding to (a), (b), (c) and (d) in Figure 8)

regions with high geostress and relatively more energy released when macroscopic failures or damages occur. This characteristic of the absolute *b*-value provides a supplementary tool for rock stress estimation. More importantly, the correlation between the absolute *b*-value and the geostress enables the further *b*-value based risk management, to some extent, independent of the geostress context.

The temporal variation of the *b*-value demonstrated that the recorded MS events are directly related to the deformation process. From the two typical cases that take into account the in-situ stress, a similar trend of the considerable decrease of the statistically derived *b*-value over a certain period can be observed before large deformation. The temporal decrease of the *b*-value, seemingly independent of the environmental geostress, thus can serve as an alerting sign of the imminent rock mass large deformation. In practice, a moving linear regression between the magnitude and the frequency of MS events over a certain period is recommended to be continuously conducted to track the real-time *b*-value. An alert should be raised if the temporal variation of the *b*-value starts to see a decrease that exceeds a certain threshold, followed by effective preventive intervention to the potential deformation of the rock mass. The two cases studied herein find the approximate criterion to be the relative decrease of the *b*-value around 10 % over 10 days. This threshold can be a reference for underground rock engineering projects in the similar context regarding the scale of underground caverns.

Table 1 Evolution of *b*-value and rock mass deformation in Houziyan underground powerhouse caverns

Time	*b*-value			Deformation	
	Absolute value	Temporal incremental decrease	Temporal incremental decrease/%	Absolute displacement/mm	Temporal incremental increase/mm
Ten days before large deformation (2013-04-16/04-22)	1.0420	0.000	0	23.68	0.00
Five days before large deformation (2013-04-23/04-27)	0.8969	−0.145	−14	23.68	0.00
One day before large deformation (2013-04-28/05-01)	0.8587	−0.183	−18	24.60	0.93
Large deformation (2013-05-02/05-20)	0.8209	−0.221	−21	34.49	10.81
Ten days before large deformation (2013-07-04/07-14)	1.0833	0.000	0	16.90	0.00
Five days before large deformation (2013-07-15/07-19)	0.8385	−0.245	−23	16.92	0.02
One day before large deformation (2013-07-20/07-23)	0.8257	−0.258	−24	16.96	0.06
Large deformation (2013-07-24/07-28)	0.7191	−0.364	−34	23.30	6.40
Ten days before large deformation (2013-11-10/11-26)	1.1103	0.000	0	6.73	0.00
Five days before large deformation (2013-11-27/11-31)	0.9727	−0.138	−12	7.24	0.51
One day before large deformation (2013-12-01/12-04)	0.6860	−0.424	−38	7.91	1.18
Large deformation (2013-12-05/12-15)	0.6768	−0.434	−39	15.81	9.08
Ten days before large deformation (2013-12-12/12-23)	1.1515	0.000	0	128.27	0.00
Five days before large deformation (2013-12-24/12-28)	1.1499	−0.002	−1	128.55	0.28
One day before large deformation (2013-12-29/2014-01-01)	0.9293	−0.222	−19	128.32	0.05
Large deformation (2014-01-02/01-10)	0.8558	−0.296	−26	146.86	18.59

5 Conclusions

1) The MS monitoring technique was applied to two large underground powerhouse caverns at different stress levels to study the MS clusters associated with rock mass large deformation. The comparison between the MS *b*-values of the two distinct underground caverns shows that the *b*-value was less than 1.0 at the high geostress level while more than 1.5 at the low geostress level. This indicated that high-magnitude MS events occurred more frequently in high stress underground caverns while low-magnitude MS events were dominant in low stress underground caverns. Furthermore, the temporal variation of the MS *b*-values and rock mass deformation monitored at both underground caverns highlighted an incremental decrease of the MS *b*-value over 10% within ten days before any imminent rock mass large deformation.

2) The present work demonstrates that the real-time *b*-value is an important and reliable index of an early-warning system for the risk management of the rock mass large deformation, on account of (a) the nature of the microseismicity and its correlation with the microfracturing in rock mass; (b) the accessibility of the *b*-value in practical use that benefits from the rapidly developing monitoring and analysing techniques; (c) the correlation between the absolute *b*-value and the geostress; and (d) the temporal variation of the *b*-value as an indicator of the imminent rock mass large deformation. Further studies are warranted to practically validate this early-warning mechanism of the *b*-value for the

Table 2 Evolution of the *b*-value and rock mass deformation in Wudongde underground powerhouse caverns

Time	*b*-value			Deformation	
	Absolute value	Temporal incremental decrease	Temporal incremental decrease/%	Absolute displacement/mm	Temporal incremental increase/mm
Ten days before large deformation (2015-08-01/08-31)	1.8505	0.000	0	18.07	0.00
Five days before large deformation (2015-09-01/09-05)	1.6180	−0.233	−13	18.05	−0.02
One day before large deformation (2015-09-06/09-09)	1.5423	−0.308	−17	18.24	0.17
Large deformation (2015-09-10/09-20)	1.3762	−0.474	−26	29.70	11.63
Ten days before large deformation (2015-08-20/09-14)	1.7535	0.000	0	2.32	0.00
Five days before large deformation (2015-09-15/09-19)	1.6782	−0.075	−4	3.18	0.86
One day before large deformation (2015-09-20/09-23)	1.5315	−0.222	−13	3.25	0.93
Large deformation (2015-09-24/09-30)	1.3838	−0.370	−21	8.66	6.34
Ten days before large deformation (2015-11-11/11-31)	2.2199	0.000	0	2.78	0.00
Five days before large deformation (2015-12-01/12-05)	1.9084	−0.312	−14	2.83	0.05
One day before large deformation (2015-12-06/12-09)	1.5693	−0.651	−29	2.86	0.08
Large deformation (2015-12-10/12-31)	1.5370	−0.683	−31	6.10	3.32
Ten days before large deformation (2016-05-10/05-30)	1.6047	0.000	0	0.16	0.00
Five days before large deformation (2016-05-31/06-04)	1.2487	−0.356	−22	0.15	−0.01
One day before large deformation (2016-06-05/06-08)	1.2217	−0.383	−24	0.20	0.04
Large deformation (2016-06-09/06-25)	1.0758	−0.529	−33	6.15	5.99

management of the geological risk, and to establish a generalized or otherwise project-oriented criterion for a wide range of geotechnical projects associated with rock mass deformation.

Contributors

LI Biao conducted the literature review and wrote the first draft of the manuscript. DING Quan-fu processed the monitoring data. Nu-wen XU edited the draft of the manuscript. DAI Feng developed the overarching research goals. XU Yuan analysed the *b*-value characteristics and edited the draft of the manuscript. QU Hong-lue summarized geological information of the engineering. All authors replied to reviewers' comments and revised the final version.

Conflict of interest

LI Biao, DING Quan-fu, XU Nu-wen, DAI Feng, XU Yuan, QU Hong-lue declare that they have no conflict of interest.

References

[1] LAI X P, CAI M F, XIE M W. In situ monitoring and analysis of rock mass behavior prior to collapse of the main transport roadway in Linglong Gold Mine, China [J]. International Journal of Rock Mechanics and Mining Sciences, 2006, 43(4): 640 − 646. DOI: 10.1016/j.ijrmms.2005.09.015.

[2] LI Zhen-lei, DOU Lin-ming, WANG Gui-feng, et al. Risk evaluation of rock burst through theory of static and dynamic stresses superposition [J]. Journal of Central South University, 2015, 22(2): 676−683. DOI: 10.1007/s11771-015-2570-2.

[3] TANG Li-zhong, XIA K W. Seismological method for prediction of areal rockbursts in deep mine with seismic source mechanism and unstable failure theory [J]. Journal of Central South University of Technology, 2010, 17(5): 947−953. DOI: 10.1007/s11771-010-0582-5.

[4] MA K, TANG C A, WANG L X, et al. Stability analysis of underground oil storage Caverns by an integrated numerical and microseismic monitoring approach [J]. Tunnelling and Underground Space Technology, 2016, 54: 81 − 91. DOI: 10.1016/j.tust.2016.01.024.

[5] STORK A L, VERDON J P, KENDALL J M. The microseismic response at the in Salah Carbon Capture and Storage (CCS) site [J]. International Journal of Greenhouse Gas Control, 2015, 32: 159−171. DOI: 10.1016/j.ijggc.2014.11.014.

[6] CAI M, KAISER P K, MARTIN C D. Quantification of rock mass damage in underground excavations from microseismic event monitoring [J]. International Journal of Rock Mechanics and Mining Sciences, 2001, 38(8): 1135 − 1145. DOI: 10.1016/S1365-1609(01)00068-5.

[7] CAI M, KAISER P K. Assessment of excavation damaged zone using a micromechanics model [J]. Tunnelling and Underground Space Technology, 2005, 20(4): 301−310. DOI: 10.1016/j.tust.2004.12.002.

[8] DAI Feng, LI Biao, XU Nu-wen, et al. Deformation forecasting and stability analysis of large-scale underground powerhouse Caverns from microseismic monitoring [J]. International Journal of Rock Mechanics and Mining Sciences, 2016, 86: 269−281. DOI: 10.1016/j.ijrmms.2016.05.001.

[9] LI Biao, XU Nu-wen, DAI Feng, et al. Dynamic analysis of rock mass deformation in large underground Caverns considering microseismic data [J]. International Journal of Rock Mechanics and Mining Sciences, 2019, 122: 104078. DOI: 10.1016/j.ijrmms.2019.104078.

[10] MA Ke, TANG Chun-an, XU Nu-wen, et al. Failure precursor of surrounding rock mass around cross tunnel in high-steep rock slope [J]. Journal of Central South University, 2013, 20(1): 207−217. DOI: 10.1007/s11771-013-1478-y.

[11] FENG Guang-liang, FENG Xia-ting, CHEN Bing-rui, et al. Effects of structural planes on the microseismicity associated with rockburst development processes in deep tunnels of the Jinping-II Hydropower Station, China [J]. Tunnelling and Underground Space Technology, 2019, 84: 273 − 280. DOI: 10.1016/j.tust.2018.11.008.

[12] XU Nu-wen, TANG Chu-nan, LI Hong, et al. Excavation-induced microseismicity: Microseismic monitoring and numerical simulation [J]. Journal of Zhejiang University: Science A, 2012, 13(6): 445 − 460. DOI: 10.1631/jzus.a1100131.

[13] HUDYMA M, POTVIN Y H. An engineering approach to seismic risk management in hardrock mines [J]. Rock Mechanics and Rock Engineering, 2010, 43(6): 891 − 906. DOI: 10.1007/s00603-009-0070-0.

[14] GUTENBERG B, RICHTER C F. Frequency of earthquakes in California [J]. Bulletin of the Seismological Society of America, 1944, 34(4): 185 − 188. DOI: 10.1785/bssa0340040185.

[15] BORMANN P. Are new data suggesting a revision of the current M_w and M_e scaling formulas? [J]. Journal of Seismology, 2015, 19(4): 989 − 1002. DOI: 10.1007/s10950-015-9507-y.

[16] AKI K. Seismic displacements near a fault [J]. Journal of Geophysical Research, 1968, 73(16): 5359 − 5376. DOI: 10.1029/JB073i016p05359.

[17] ZHANG Peng-hai, YANG Tian-hong, YU Qing-lei, et al. Microseismicity induced by fault activation during the fracture process of a crown pillar [J]. Rock Mechanics and Rock Engineering, 2015, 48(4): 1673 − 1682. DOI: 10.1007/s00603-014-0659-9.

[18] WYSS M, SHIMAZAKI K, WIEMER S. Mapping active magma Chambers by *b* values beneath the off-Ito volcano, Japan [J]. Journal of Geophysical Research: Solid Earth, 1997, 102(B9): 20413−20422. DOI: 10.1029/97JB01074.

[19] AMELUNG F, KING G. Earthquake scaling laws for creeping and non-creeping faults [J]. Geophysical Research Letters, 1997, 24(5): 507−510. DOI: 10.1029/97GL00287.

[20] WIEMER S, MCNUTT S R, WYSS M. Temporal and three-dimensional spatial analyses of the frequency-magnitude distribution near Long Valley Caldera, California [J]. Geophysical Journal International, 1998, 134(2): 409 − 421. DOI: 10.1046/j.1365-246x.1998.00561.x.

[21] SCHORLEMMER D, WIEMER S, WYSS M. Variations in earthquake-size distribution across different stress regimes [J]. Nature, 2005, 437(7058): 539 − 542. DOI: 10.1038/nature04094.

[22] WIEMER S, WYSS M. Mapping the frequency-magnitude distribution in asperities: An improved technique to calculate recurrence times? [J]. Journal of Geophysical Research: Solid Earth, 1997, 102(B7): 15115 − 15128. DOI: 10.1029/97JB00726.

[23] KHAN P K, CHAKRABORTY P P. The seismic *b*-value and its correlation with Bouguer gravity anomaly over the Shillong Plateau area: Tectonic implications [J]. Journal of Asian Earth Sciences, 2007, 29(1): 136−147. DOI: 10.1016/j.jseaes.2006.02.007.

[24] MOUSAVI S M. Mapping seismic moment and *b*-value within the continental-collision orogenic-belt region of the Iranian Plateau [J]. Journal of Geodynamics, 2017, 103: 26−41. DOI: 10.1016/j.jog.2016.12.001.

[25] BORA D K, BORAH K, MAHANTA R, et al. Seismic *b*-values and its correlation with seismic moment and Bouguer gravity anomaly over Indo-Burma ranges of northeast India: Tectonic implications [J]. Tectonophysics, 2018, 728 − 729: 130−141. DOI: 10.1016/j.tecto.2018.01.001.

[26] KULHANEK O, PERSSON L, NUANNIN P. Variations of *b*-values preceding large earthquakes in the shallow subduction zones of Cocos and Nazca plates [J]. Journal of South American Earth Sciences, 2018, 82: 207−214. DOI: 10.1016/j.jsames.2018.01.005.

[27] LEGGE N, SPOTTISWOODE S. Fracturing and microseismicity ahead of a deep gold mine stope in the pre-remnant and remnant stages of mining [C]// 6th ISRM Congress, Montreal, Canada, 1987: 2071−1048.

[28] LIU Jian-po, FENG Xia-ting, LI Yuan-hui, et al. Studies on temporal and spatial variation of microseismic activities in a deep metal mine [J]. International Journal of Rock

Mechanics and Mining Sciences, 2013, 60: 171－179. DOI: 10.1016/j.ijrmms.2012.12.022.

[29] LU Cai-ping, LIU Guang-jian, LIU Yang, et al. Microseismic multi-parameter characteristics of rockburst hazard induced by hard roof fall and high stress concentration [J]. International Journal of Rock Mechanics and Mining Sciences, 2015, 76: 18－32. DOI: 10.1016/j.ijrmms.2015.02.005.

[30] MA X, WESTMAN E, SLAKER B, et al. The *b*-value evolution of mining-induced seismicity and mainshock occurrences at hard-rock mines [J]. International Journal of Rock Mechanics and Mining Sciences, 2018, 104: 64－70. DOI: 10.1016/j.ijrmms.2018.02.003.

[31] Ministry of Water Resources of the People's Republic of China. GB50287-99. Code for water resource and hydropower engineering geological investigation [S]. 1999, 82p. (in Chinese)

[32] SJÖBERG J, CHRISTIANSSON R, HUDSON J A. ISRM suggested methods for rock stress estimation—Part 2: Overcoring methods [J]. International Journal of Rock Mechanics and Mining Sciences, 2003, 40(7, 8): 999－1010. DOI: 10.1016/j.ijrmms.2003.07.012.

[33] SUGAWARA K, OBARA Y. Draft ISRM suggested method for in situ stress measurement using the compact conical-ended borehole overcoring (CCBO) technique [J]. International Journal of Rock Mechanics and Mining Sciences, 1999, 36(3): 307−322.

[34] CHENG Li-juan, LI Zhi-guo, WANG Jin-sheng, WANG Di-kai, XIA Xin. Design report on reinforcement measures for surrounding rock mass in underground group caverns of the Houziyan Hydropower Station along Dadu River [R]. HydroChina Chengdu Engineering Corporation, Chengdu, China, 2014: 1−163. (in Chinese)

[35] STOCKWELL R G, MANSINHA L, LOWE R P. Localization of the complex spectrum: The S transform [J]. IEEE Transactions on Signal Processing, 1996, 44(4): 998－1001. DOI: 10.1109/78.492555.

[36] HAIMSON B C, CORNET F H. ISRM Suggested Methods for rock stress estimation—Part 3: Hydraulic fracturing (HF) and/or hydraulic testing of pre-existing fractures (HTPF) [J]. International Journal of Rock Mechanics and Mining Sciences, 2003, 40(7, 8): 1011−1020. DOI: 10.1016/j.ijrmms.2003.08.002.

[37] ZHANG Cun-hui, LIU Hui-bo, ZHANG Ling-li. Stability evaluation and supports design optimization for surrounding rock mass in underground powerhouse caverns at the Wudongde Hydropower Station along Jinsha River [R]. Changjiang Institute of Survey, Planning, Design and Research, Wuhan, China, 2015: 57−61. (in Chinese)

[38] LI Ang, XU Nu-wen, DAI Feng, et al. Stability analysis and failure mechanism of the steeply inclined bedded rock masses surrounding a large underground opening [J]. Tunnelling and Underground Space Technology, 2018, 77: 45−58. DOI: 10.1016/j.tust.2018.03.023.

[39] LI Ang, LIU Yi, DAI Feng, et al. Continuum analysis of the structurally controlled displacements for large-scale underground Caverns in bedded rock masses [J]. Tunnelling and Underground Space Technology, 2020, 97: 103288. DOI: 10.1016/j.tust.2020.103288.

[40] WOESSNER J. Assessing the quality of earthquake catalogues: Estimating the magnitude of completeness and its uncertainty [J]. Bulletin of the Seismological Society of America, 2005, 95(2): 684−698. DOI: 10.1785/0120040007.

[41] GREENHOUGH J, MAIN I G. A Poisson model for earthquake frequency uncertainties in seismic hazard analysis [J]. Geophysical Research Letters, 2008, 35(19): L19313. DOI: 10.1029/2008GL035353.

[42] LIU Xi-ling, HAN Meng-si, HE Wei, et al. A new *b* value estimation method in rock acoustic emission testing [J]. Journal of Geophysical Research: Solid Earth, 2020, 125(12): e2020JB019658. DOI: 10.1029/2020JB019658.

[43] XU Yuan, DAI Feng. Dynamic response and failure mechanism of brittle rocks under combined compression-shear loading experiments [J]. Rock Mechanics and Rock Engineering, 2018, 51(3): 747－764. DOI: 10.1007/s00603-017-1364-2.

[44] LIU Yi, DAI Feng, DONG Lu, et al. Experimental investigation on the fatigue mechanical properties of intermittently jointed rock models under cyclic uniaxial compression with different loading parameters [J]. Rock Mechanics and Rock Engineering, 2018, 51(1): 47−68. DOI: 10.1007/s00603-017-1327-7.

[45] FENG Guang-liang, FENG Xia-ting, CHEN Bing-rui, et al. Characteristics of microseismicity during breakthrough in deep tunnels: Case study of Jinping-II hydropower station in China [J]. International Journal of Geomechanics, 2020, 20(2): 04019163. DOI: 10.1061/(asce)gm.1943-5622.0001574.

[46] XU Y, DAI F, XU N W, et al. Numerical investigation of dynamic rock fracture toughness determination using a semi-circular bend specimen in split Hopkinson pressure bar testing [J]. Rock Mechanics and Rock Engineering, 2016, 49(3): 731−745. DOI: 10.1007/s00603-015-0787-x.

[47] DONG Long-jun, WESSELOO J, POTVIN Y, et al. Discrimination of mine seismic events and blasts using the fisher classifier, naive Bayesian classifier and logistic regression [J]. Rock Mechanics and Rock Engineering, 2016, 49(1): 183−211. DOI: 10.1007/s00603-015-0733-y.

[48] DONG Long-jun, ZOU Wei, LI Xi-bing, et al. Collaborative localization method using analytical and iterative solutions for microseismic/acoustic emission sources in the rockmass structure for underground mining [J]. Engineering Fracture Mechanics, 2019, 210: 95−112. DOI: 10.1016/j.engfracmech.2018.01.032.

(Edited by HE Yun-bin)

中文导读

不同应力水平下地下厂房洞室群围岩大变形微震*b*值特征

摘要：地下厂房洞室群围岩大变形已成为中国西南地区水电工程的严重灾害，围岩大变形孕育过程中将产生一系列的岩石破裂，运用微震监测技术可监测到这些破裂信息。在地应力水平不同的两个典型地下厂房洞室群构建精度微震监测系统，分析了围岩大变形微震*b*值及其时间变化特征。结果表明，高地应力地下厂房洞室群围岩大变形过程微震*b*值小于1.0，而低地应力情况下微震*b*值大于1.5。对于高、低地应力地下厂房洞室群而言，围岩大变形前十日内， 微震*b*值均出现超过10%的下降。研究成果有助于提高围岩大变形微震震源破裂特征的认识，也可为地下厂房洞室群围岩大变形预警提供重要参考。

关键词：地下厂房洞室群；围岩大变形；应力水平；微震监测；*b*值